

Article

Corrosion Behavior of Hybrid Zinc Coatings Based on Chitosan and Corrosion Inhibitor BTA: Effect of the Molecular Weight and ζ -Potential

Viktoria Milkova ¹, Nelly Boshkova ¹, Georgy Grancharov ², Olya Stoilova ²  and Nikolai Boshkov ^{1,*} 

¹ Institute of Physical Chemistry "R. Kaishev", Bulgarian Academy of Sciences, 1113 Sofia, Bulgaria; vmilkova@ipc.bas.bg (V.M.); nelly.boshkova@ipc.bas.bg (N.B.)

² Institute of Polymers, Bulgarian Academy of Sciences, 1113 Sofia, Bulgaria; granchar@polymer.bas.bg (G.G.); stoilova@polymer.bas.bg (O.S.)

* Correspondence: nboshkov@ipc.bas.bg

Abstract: The creation of anticorrosion hybrid zinc-based coatings containing chitosan particles with low (LMC) or high (HMC) molecular weight is an effective method for safe and durable exploitation of different steel infrastructures. In this work, hybrid coatings consisting of zinc and two types of chitosan particles (LMC or HMC) were obtained to protect low-carbon steel from corrosion attack in a chloride environment. Chitosans with different molecular weights (CS50 Mw 50–190 kDa and CS190 Mw 190–310 kDa) have been applied. Furthermore, both particle types were prepared with or without additional content of incorporated corrosion inhibitor benzotriazole (BTA). The chitosan particles were obtained and thereafter electrodeposited in the form of hybrid coatings on mild steel substrates. The electrokinetic charge and hydrodynamic size of the particles and the stability of their aqueous suspensions were evaluated using dynamic light scattering. The concentration of BTA loaded into the particles was determined by the difference between the initial concentration of the compound added during the particle preparation and the concentration in the supernatant after centrifugation of the dispersion. The hybrid coatings were compared concerning their surface morphology, topography, and hydrophilicity (SEM and AFM analysis, water contact angle measurement) as well as corrosion and electrochemical behavior (potentiodynamic polarization curves—PD, polarization resistance—Rp, cyclic voltammetry—CVA). The protective characteristics of the coatings were studied in 5% NaCl solution. The results obtained from the PD studies demonstrated lower corrosion current densities of all hybrid coatings compared to the ordinary zinc one. In addition, the Rp tests showed enhanced protective ability and corrosion resistance of LMC and LMCB compared to the ordinary zinc, HMC, and HMCB, respectively. The obtained scientific information presented the effect of the molecular weight and ζ -potential of the particles on the anticorrosion ability of the hybrid coatings compared to the ordinary zinc one.



Citation: Milkova, V.; Boshkova, N.; Grancharov, G.; Stoilova, O.; Boshkov, N. Corrosion Behavior of Hybrid Zinc Coatings Based on Chitosan and Corrosion Inhibitor BTA: Effect of the Molecular Weight and ζ -Potential. *Coatings* **2024**, *14*, 495. <https://doi.org/10.3390/coatings14040495>

Academic Editors: Henryk Kania, Florence Lequien and Anželina Marek

Received: 29 March 2024

Revised: 12 April 2024

Accepted: 14 April 2024

Published: 17 April 2024



Copyright: © 2024 by the authors. Licensee MDPI, Basel, Switzerland. This article is an open access article distributed under the terms and conditions of the Creative Commons Attribution (CC BY) license (<https://creativecommons.org/licenses/by/4.0/>).

1. Introduction

Chitosans are polysaccharides obtained by deacetylation of chitin—one of the most abundant polysaccharides in nature. Chitosan is a linear polysaccharide composed of randomly distributed β -(1-4)-2-acetamido-2-deoxy- β -D-glucopyranose and 2-amino-2-deoxy- β -D-glucopyranose unit [1,2]. The presence of NH₂-functional groups along the polymer chain determines its polyelectrolyte properties. The polycationic behavior of chitosan enables the formation of complexes with oppositely charged biomolecules, particles, or lipid membranes [3–7]. Chitosan charge density is pH-dependent, which is beneficial for various biotechnological applications. It is well known that chitosans are completely natural, biocompatible, and biodegradable polymers having a gel-forming capability and

high adsorption capacity with potential pharmaceutical and medical applications. In addition, very recently it was shown that chitosan can be used also as an effective anticorrosion agent [8–10].

Chitosan-based (CS) particles are promising delivery systems in biotechnology, medicine, or pharmacy. They can be produced by using different methods (emulsification, solvent diffusion, ionic gelation) but among them, the ionotropic gelation process or ion-induced gelation is one of the most used methods for particle formation [11,12]. The method is preferred because of the application of mild conditions achieved without applying organic solvents. The method consists of a spontaneous sol-gel transition of chitosan in the presence of a polyanionic crosslinking agent, typically sodium tripolyphosphate (TPP). The complex is stabilized by cross-linked electrostatic interaction between NH_3^+ groups of chitosan and O^- groups of TPP, resulting in a three-dimensional matrix that precipitates from an aqueous solution in the form of gel-like particles [13,14]. Due to the pH-dependent charge density of chitosan, the CS-TPP particles are synthesized in a dilute aqueous acidic solution. The presence of an excess of a positive charge of the particles allows the incorporation of negatively charged molecules (proteins, drugs, or enzymes). In the literature, there are well-established protocols for the preparation of the particles and systematic investigation of the effect of different factors (initial polymer concentration, chitosan to TPP molar ratio, degree of acetylation of the chitosan, presence of salts in the medium) on the properties of the produced structures [15–17].

It is well known that the corrosion of the metal and alloy structures may cause serious economic costs as well as safety and environmental problems. In order to make comparisons between countries in terms of corrosion costs, the latter are usually expressed as a share of the country's gross domestic product (GDP). Generally, the global cost of corrosion can be estimated as more than USD 2.5 trillion. This sum is about 3%–5% of the global GDP. These costs also include environmental consequences like misses, incidents, forced shutdowns (outages), accidents, etc. The lack of corrosion management can be very costly. On the other hand, the cost of the US alone to cover corrosion damage is about USD 500 billion each year (about 3.1% of US GDP). To some extent, the situation is similar for Europe, where the estimated direct costs of corrosion were around EUR 250 billion until a few years ago. Research conducted using different methodology in Great Britain and Australia has reached similar estimates of corrosion damage, i.e., that the latter are between 1 and 5% of each country's GDP. It is also known that about 10% of the annual metal extraction remains as irrecoverable loss.

This dangerous event is often induced by chloride ions [18]. Their action generally leads to destruction of buildings, bridges, railway facilities, etc. and requires significant financial costs to increase the corrosion resistance and to minimize the possible negative effects. The application of additionally protected low-carbon steels with different coating types (metallic, hybrid, conversion etc.) gives one opportunity due to their relatively lower cost, good mechanical strength, and other parameters. One economically viable approach for better protection of low-carbon steel is galvanizing [19,20]. In general, there is no doubt that the surface modification of the base metal with protective coatings is an effective method of obtaining better anticorrosion performance. Zinc and zinc-based alloy coatings are applied for corrosion protection, especially of low-carbon steel due to the fact that zinc is more active than iron and plays a sacrificial role in the case of corrosion attack [21,22]. Particularly, the corrosion process on bare zinc coatings leads to the formation of so-called "white rust" [22,23]. The modern tendency is to replace the bare zinc coatings with composite or hybrid ones [23,24]. For example, the incorporation of different metal, oxide, polymer, or other particles enhances the protective characteristics of the ordinary zinc coatings. The reason for this statement is the formation of "mixed" barrier layers, the latter containing corrosion products with low solubility and the incorporated particles [24–26].

The present study is focused on the investigation of the combined anticorrosion effect of chitosan with different physicochemical characteristics and those of the benzotriazole (BTA)—a compound with a prominent anticorrosion activity. For this purpose, stable

spherical chitosan-based particles loaded with BTA were produced. Further, the obtained chitosan particles were electrodeposited in hybrid coatings on low carbon steel substrates to protect them from corrosion attack in chloride environment. Finally, the effect of the molecular weight of chitosan and ζ -potential of the particles on the anticorrosion ability were evaluated compared to ordinary zinc coating.

2. Materials and Methods

2.1. Materials and Preparation Procedure

All reagents used for preparation of composite particles were purchased from Sigma-Aldrich (St. Louis, MO, USA). Chitosans with a degree of deacetylation DDA 75%–85% and different molecular weights (CS50 Mw 50–190 kDa and CS190 Mw 190–310 kDa) were chosen for this study. The stock solutions were prepared with 2 mg/mL of acetic acid and filtered through a 0.45 μm filter (Minisart[®], Sartorius, Göttingen, Germany) to remove possible aggregates and impurities. The stock solutions of sodium tripolyphosphate (TPP, 1 mg/mL) and benzotriazole (BTA, 10 mg/mL) were prepared in double distilled water.

2.2. Methods—Particle Synthesis

The chitosan particles were formed according to the procedure proposed by Calvo et al. [11]. The solution of TPP (2 mL) was dropped into the chitosan solution (3 mL) under uninterrupted stirring for 10 min. The mass ratio between the chitosan and TPP was 3:1. The particles loaded with corrosion inhibitor were produced by using almost the same procedure, but the solution of TPP (2 mL) was added to the mixture of chitosan solution (3 mL) and BTA (3 mL) under vigorous stirring for 10 min. The produced chitosan particles were kept at room temperature for at least 1 h.

In order to study the stability of the particles at conditions close to ones in electrochemical studies, the particles were isolated through centrifugation at 15,000 rpm (21,382 g) and 15 °C for 90 min using a laboratory centrifuge (PW-352R, MPW Med.Instruments, Warsaw, Poland). The settled particles were re-dispersed in phosphate buffer pH 7 (Chem-Lab NV, Zedelgem, Belgium). Moreover, the stability of the particles was evaluated by mixing the maternal solution of particles and buffer pH 7 in ratio 1:1.

2.3. Characterization of the Electrokinetic Charge and Size of the Composite Liposomes

The overcompensation of the electrokinetic charge and hydrodynamic size (diameter) of the produced particles were evaluated by using dynamic light scattering with non-invasive backscattering (DLS-NIBS, measuring angle 173°).

The ζ -potential was determined by mixed-mode measurement phase-analysis light scattering. Dynamic light scattering measurements were carried out using Zetasizer Pro (Malvern Panalytical Ltd., Malvern, UK) equipped with a He-Ne laser with a maximum power of 10 mW operating at a wavelength of 633 nm with a fixed scattering light angle of 173°. All measurements were performed at 24.0 ± 0.1 °C. After five measurements, the average value was taken as the electrokinetic charge and size of the capsules.

2.4. Determination of the Encapsulated Amount of Corrosion Inhibitor

The concentration of BTA loaded into the particles was determined by the difference between the initial concentration of the compound added during the particle preparation and the concentration in the supernatant after centrifugation of the dispersion by monitoring with JenwayTM 6305 UV/Visible Spectrophotometer (Bibby Scientific Limited, Staffordshire, UK).

The inhibitor was detected at a wavelength of 260 nm corresponding to the maximum absorbance peak in BTA spectra. The amount of free BTA in the solution was calculated by using an appropriate calibration curve. The encapsulation efficiency (EE%) was estimated by using

$$\text{EE\%} = \frac{C_{\text{total}} - C_{\text{free}}}{C_{\text{total}}} \times 100 \quad (1)$$

where the C_{total} is the initial concentration of the BTA (3.75 mg/mL) and C_{free} is the calculated concentration of the compound in the supernatant.

2.5. Stability of the Uploaded and BTA-Loaded Particles at the Corrosion Conditions

The conditions close to the ones in the corrosion experiment were simulated to determine the behavior of the particles. Two procedures were performed to evaluate the stability of the dispersion of the particles. In the first procedure, aliquots (4 Eppendorf tubes of 5 mL) from the dispersion were centrifuged (at 15,000 rpm and 15 °C for 90 min). The supernatants were removed, and the settled particles were re-dispersed in the same volume buffer pH 7 (Chem-Lab NV, Zedelgem, Belgium) by sonication (10 min in an ultrasonic bath). In the second procedure, the dispersion of particles and buffer pH 7 were mixed in a ratio of 1:1. The comparison in size and ζ -potential of the particles before and after the addition of a buffer was evaluated 24 h after mixing. The released amount of BTA was determined by UV-vis spectroscopy. For this purpose, the samples were centrifuged and the concentration of the compound was estimated by using an appropriate calibration curve.

2.6. Transmission Electron Microscopy (TEM)

The produced capsules were visualized by TEM. The samples for the TEM studies were prepared by dropping and drying a drop of suspension of capsules on formvar-covered TEM grids. The images were captured using a high-resolution scanning transmission electron microscope HR STEM JEOL JEM 2100 (JEOL Ltd., Tokyo, Japan) for investigations of surface morphology.

2.7. Electrodeposition of Hybrid Coatings with Incorporated Chitosan Particles of Low- and High-Polymer Molecular Weight

The electrodeposition process of zinc and hybrid zinc-based coatings is performed on low-carbon steel plates (sizes 2 cm × 1 cm × 0.1 cm) from a slightly acidic electrolyte (pH value 4.5–5.0) containing 150 g/L ZnSO₄·7H₂O, 30 g/L NH₄Cl, and 30 g/L H₃BO₃ as well as two additives—wetting agent AZ1 (50 mL/L) and brightener AZ2 (mL/L). A glass cell with 600 mL electrolyte volume was applied at room temperature, cathode current (DC current) density of 2 A/dm², and usage of soluble zinc anodes. The thickness of all the coatings obtained was ~12 µm. After removing the samples from the electrolyte bath, they were dried in air. The concentration of both chitosan particle types in the starting electrolytes was 10⁻² g/L. The obtained hybrid coatings are designated as follows: LMC—coatings with incorporated low molecular chitosan particles; LMCB—coatings with incorporated low molecular chitosan particles with entrapped BTA; HMC—coatings with incorporated high molecular chitosan particles; HMBC—coatings with incorporated high molecular chitosan particles with entrapped BTA.

2.8. Surface Morphology

Surface morphology and distribution of the incorporated chitosan particles, LMC or HMC, respectively, in the hybrid coatings were evaluated by application of scanning electron microscopy (INCA Energy 350 unit, Oxford, UK).

2.9. Corrosion Characterization and CVA Studies

The protective properties and electrochemical characteristics of the hybrid coatings obtained were evaluated with selected methods like potentiodynamic (PDP) polarization curves and polarization resistance (Rp) measurements. Their corrosion parameters were compared with these of ordinary zinc coating. The cathodic deposition and anodic dissolution processes were investigated with Cyclic Voltammetry (CVA) directly in the starting electrolytes.

These investigations were realized with computerized PAR unit "VersaStat 4" (Princeton Applied Research, Princeton, NJ, USA). During the tests, a Saturated Calomel Electrode (SCE) was applied as a reference while a platinum plate was the counter electrode. The

PDP curves were stopped after visual observation of the steel substrate checked by “naked eye”. The Rp measurements had a duration of 45 days. Cyclic voltammetry (CVA) studies were pursued in the potential interval between -1.4 V and 0 V with a scan rate of 10 mV/s.

2.10. Atomic Force Microscopy (AFM) and Water Contact Angle Measurements

AFM imaging was performed on a Bruker Dimension Icon microscope working under standard tapping (ST) mode. The micrographs were recorded at room temperature using silicon tips (RTESPA) with resonance frequency of approximately 300 kHz and spring constant 40 N/m at the scan rate of 1.0 Hz. The water contact angles (WCAs) were evaluated using an Easy Drop DSA20E Krüss GmbH apparatus (Hamburg, Germany) at ambient temperature. A sessile droplet of distilled water (10 μ L) controlled by a computer dosing system was deposited onto the samples. The WCA was calculated by computer analysis of the images of the droplet by DSA1 software (version: V1.92-05). The data are averaged from 10 measurements for each sample.

2.11. Test Medium and Reproducibility

Electrochemical and corrosion tests were carried out in a model medium causing generally local corrosion—5% NaCl solution ($\text{pH} \sim 6.7$). The experimental results in the test medium were summarized as an average from the data obtained of five samples per type, i.e., either ordinary zinc or hybrid zinc coatings with incorporated chitosan particles of low or high molecular weight with or without incorporated inhibitor BTA.

3. Results and Discussion

3.1. Characterization of the Chitosan-TPP Particles

The visualization of the produced dispersion is presented in Figure 1. The particles are formed by the crosslinking of chitosan molecules with TPP. BTA is a weak acid (pK_a 8.2) and in the present experimental conditions, the molecules of the inhibitor are negatively charged. Therefore, it was supposed that the incorporation of BTA in the polymer matrix is governed predominantly by the electrostatic interactions with the positively charged chitosan monomers.

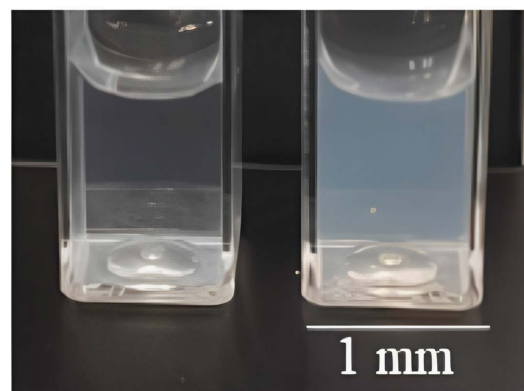


Figure 1. Dispersions of the produced BTA-loaded chitosan-based particles formed from CS190 (**left**) and CS50 (**right**).

The analysis of the characteristics of the particles indicates that the size of the unloaded particles almost does not depend on the chitosan molecular weight. Moreover, the registered diameter of the BTA-loaded particles is smaller compared to the unloaded ones (Table 1). That is why it was supposed that the decrease in the particle size results from strong electrostatic interactions between the charged components.

The registered diameters of the particles are close to the statistical estimation from TEM images (for CS-TPP particles ca. 100 nm and CS-TPP-BTA particles ca. 80 nm) presented in Table 2. The polydispersity of the sample from CS190-TPP-BTA ($\text{PDI} \sim 0.12$) is significantly higher compared to the CS190-TPP ($\text{PDI} \sim 0.31$). Moreover, the dimensions presented in

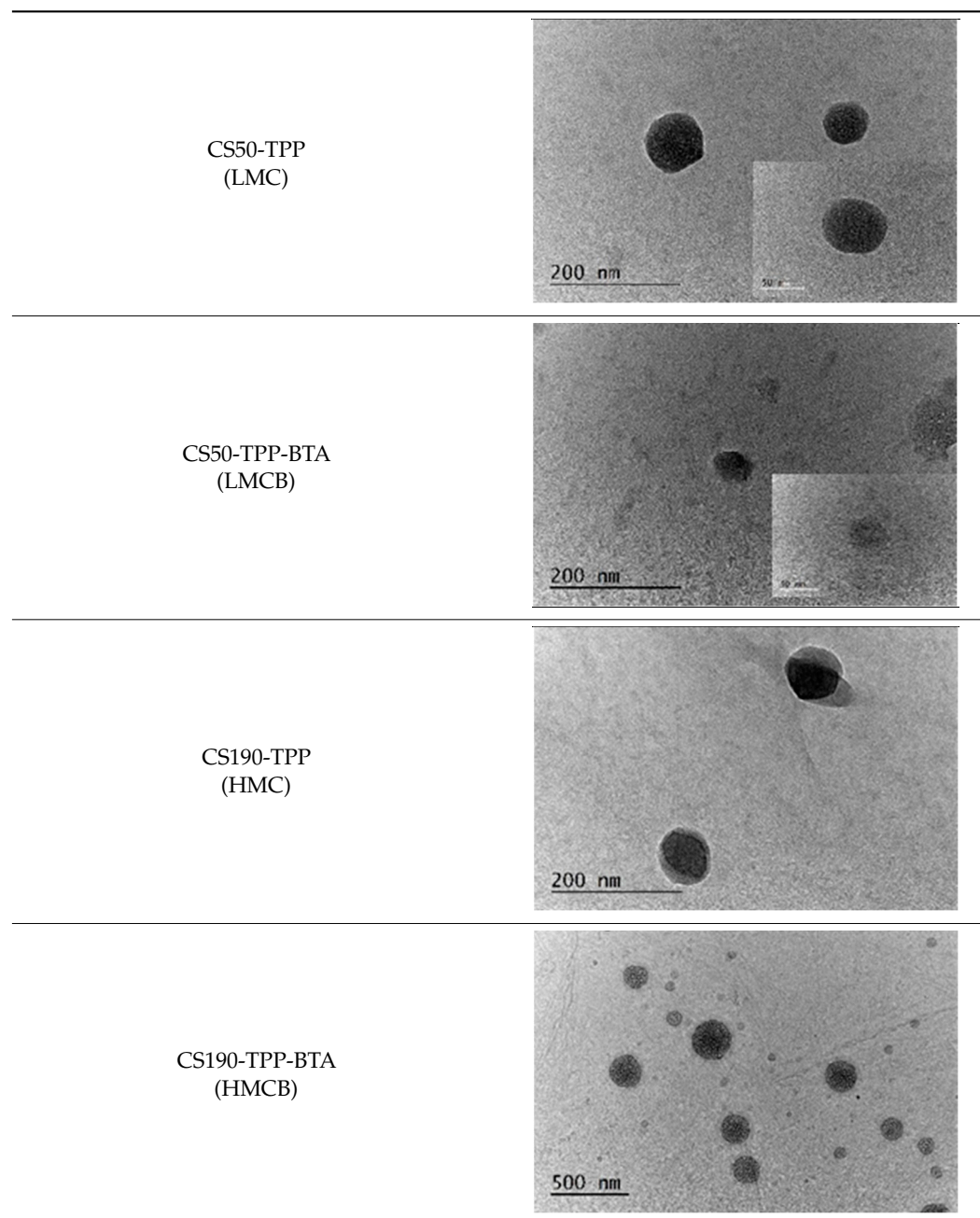
Table 1 correspond to the hydrodynamic diameter of the produced particles, which is almost two times higher compared to the real size [27].

Table 1. Characterization of the produced chitosan-based particles.

Sample	D *, nm	ζ -Potential, mV
CS50-TPP (LMC)	223.4 ± 8.20	46.8 ± 1.05
CS50-TPP-BTA (LMCB)	130.8 ± 1.85	45.9 ± 0.46
CS190-TPP (HMC)	218.7 ± 8.65	39.4 ± 0.57
CS190-TPP-BTA (HMCB)	139.8 ± 2.43	39.6 ± 0.32

* sizes are determined by a mean intensity.

Table 2. TEM images of unloaded and BTA-loaded chitosan-based particles formed from LCS and HCS (CS50 and CS190, respectively).



3.2. Estimation of the Loaded Amount from the Corrosion Inhibitor BTA

The concentration of the inhibitor loaded into the polymer particles was estimated by the values of absorbance from the supernatant after centrifugation of the particle dispersion using the calibration curve and suitable dissolution of the samples (Figure 2). According to the experimental results, the encapsulation efficiency of BTA is ca. 99% and does not depend on the molecular weight of chitosan.

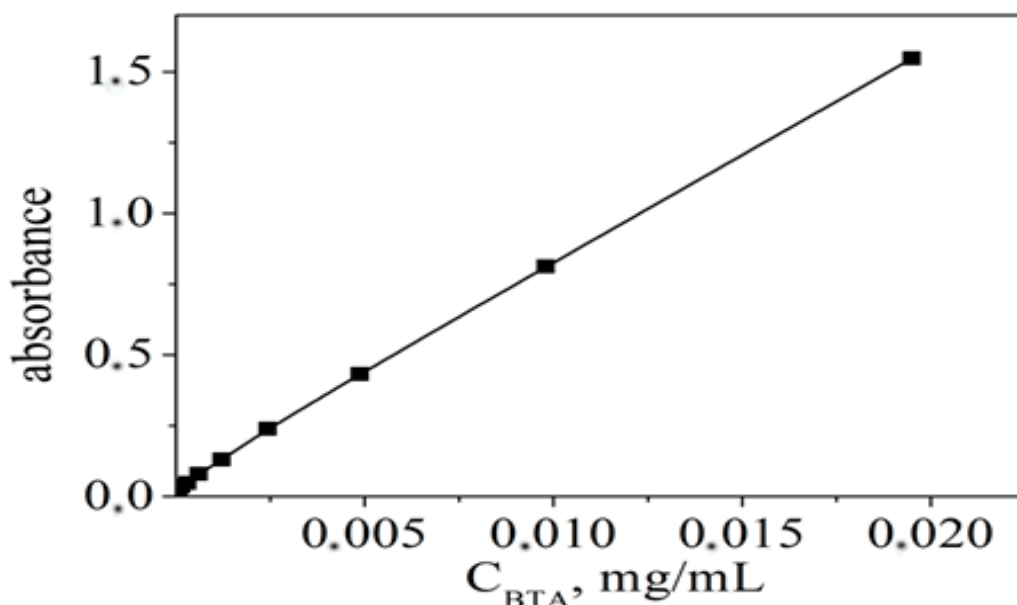


Figure 2. Calibration curve used for estimation of the concentration of BTA in buffer with pH 7 ($y = 80.79x$).

3.3. Surface Morphology

SEM micrographs of LMC and LM**C** hybrid coatings before (as received) and after corrosion treatment (immersion for 45 days in the test medium) are presented in Figure 3. It is well seen that both LMC and LM**C** demonstrated relatively uneven and partially rough surfaces. After immersion in the test medium, some individual white spheres appear on their surfaces, which seem to be the incorporated particles. The amount of the latter is much greater for the sample LMC, which is a sign for the accelerated dissolution process of the zinc as a result of the corrosion. Partially similar is the case of LM**C** hybrid coating; however, the number of the particles is reduced. Most probably, the reason for this is the presence of BTA, which hampers the zinc dissolution to a certain degree. It could be supposed that on both samples, the so-called “mixed” layer appears, the latter simultaneously containing zinc corrosion products form the dissolution process (mainly zinc hydroxide chloride ZHC, well known from other our investigations in that medium) and chitosan particles with encapsulated BTA [28–32].

SEM micrographs of the HMC and HM**C** hybrid coatings before and after corrosion treatment are demonstrated in Figure 4. Contrary to LMC and LM**C** samples, the surfaces of these hybrid coatings look more even, and some of the incorporated chitosan particles are well visible. However, after the corrosion treatment, these surfaces look much more damaged compared to LMC and LM**C** with several concaved and protruded zones after the attack of the aggressive chloride ions, i.e., their corrosion resistance is strongly decreased.

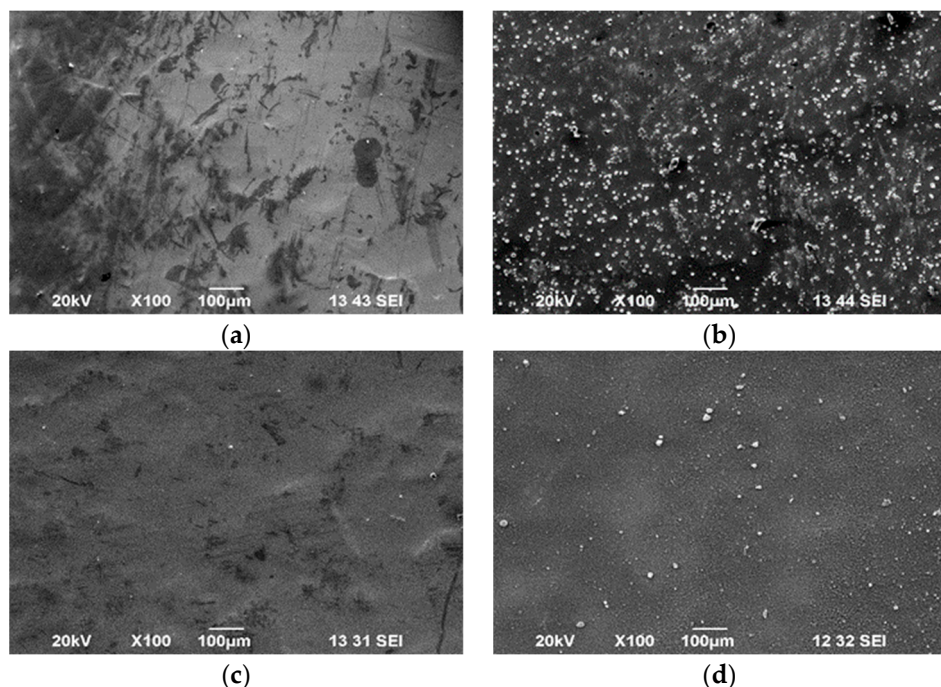


Figure 3. SEM images of hybrid LMC (a,b) and LMCB (c,d) coatings before (a,c) and after (b,d) corrosion treatment in model medium of 5% NaCl solution.

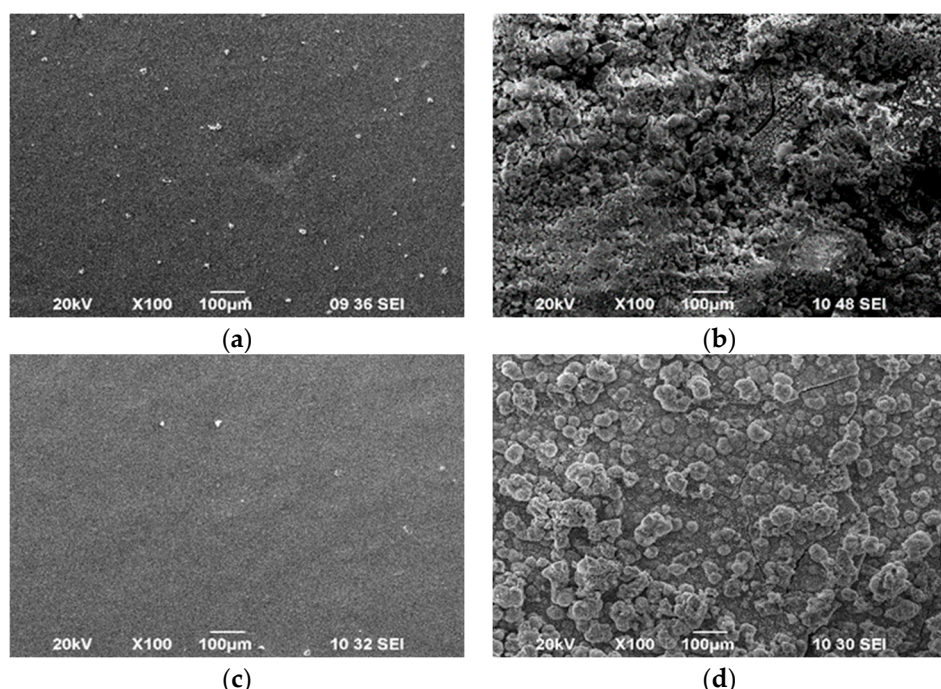


Figure 4. SEM images of hybrid HMC (a,b) and HMCCB (c,d) coatings before (a,c) and after (b,d) corrosion treatment in model medium of 5% NaCl solution.

3.4. Behavior of the Polymer Particles at the Corrosion Conditions

The determination of the stability of the dispersion at pH 7 according to the first procedure indicates an aggregation of the particles in the system. The size of the particles is ca. 4 μm , and the electrokinetic charge is very close to zero. In the second procedure, the aggregations were observed for dispersions of particles formed from low-molecular-weight chitosan (LMC) immediately after the mixing of the solutions. In the dispersion of particles formed from chitosan CS190 (HMC), significant aggregation was not observed. The

observed behavior of the dispersion is expected because of the very high ionic strength of the buffer (10^{-1} M), but the amount of inhibitor released from the particles was interesting. The concentration of free BTA in the buffer is estimated at 10^{-2} mg/mL (ca. 0.5% for 24 h) and does not depend on the chitosan characteristics or the applied procedure.

Interestingly, the characteristics and stability of the produced polymer particles are very similar despite the different physicochemical characteristics of chitosans used for their formation. According to the presented data in Table 1, the size of the BTA-loaded or unloaded particles does not depend on the chitosan. There is a difference only in the electrokinetic potential of the particles. Recently, it has been presented that the properties of CS-TPP particles strongly depend on the molar ratio of the components, degree of deacetylation, and molecular weight of chitosan [17]. In the present study, polymers with DDA ca. 20% and different molecular weights are used. Therefore, the participation of the polymer conformation effects in particle formation was supposed. The incorporation of the long molecules of the high-molecular polymer in the matrix might be suppressed and, as a result, the amount of chitosan in the matrix will be lower compared to the particles formed from a low-molecular polymer. Hence, the positive charge of the complex will be lower. Moreover, in spite of the similar properties of the particles, the dispersions of particles look different (Figure 1). It was supposed that the different conformation of the polymers and the structure characteristics of the produced particles are responsible for the observed behavior.

3.5. Cyclic Voltammetry (CVA) Studies

The results from CVA voltammetry for LMC samples with or without entrapped BTA are presented in Figure 5. The tests are realized in the starting electrolytes for electrodeposition of ordinary and both hybrid zinc coatings with or without BTA—LMC and LM**C**B hybrids, respectively. As observed, the electrodeposition process of the ordinary zinc occurs at much higher cathodic current and starts at more positive potential value compared to both hybrid coatings, i.e., the cathodic deposition of the latter is overpolarized and occurs at more negative cathodic potentials and much lower cathodic current—0.008 A for LMC sample and 0.007 A for the LM**C**B one, respectively. The anodic parts of the curves demonstrate peaks, which are characteristic for the anodic dissolution process confirming the presence of the coatings electrodeposited during the cathodic process. It is well visible that the Zn dissolution peak is the greatest one (0.065 A at -0.725 V), which is a sign of greater electrodeposited mass. Contrary to this, the anodic peaks of both hybrids are much lower—0.015 A for the LMC sample and 0.009 A for the LM**C**B one. Obviously, the presence of chitosan particles with or without BTA in the starting solutions seems to be the reason for this observation. Chitosan particles are greater in size compared to the zinc ions, and during their electrodeposition on the substrate, it is expected that they will physically block the surface for the deposition of the free zinc ions to a certain degree. The presence of BTA probably leads to an interaction with the applied additives, which results in lower cathodic current for the LM**C**B sample compared to the LMC one. The Inset in Figure 5 clearly demonstrates the cathodic and anodic parts of the processes occurring in the electrolytes for obtaining of the investigated coatings.

The results from CVA voltammetry of the HMC samples with or without entrapped BTA are shown in Figure 6. It is obvious that also here the electrodeposition process of the ordinary zinc starts at more positive potential value compared to both hybrid coatings, and the cathodic deposition of both later is overpolarized. The difference is that the electrodeposition of the hybrids occurs at lower cathodic current compared to Figure 5, i.e., 0.006 A for the HMC sample and 0.004 A for the HM**C**B one, respectively. The anodic parts of HMC and HM**C**B curves present peaks, which are lower compared to LMC and LM**C**B from Figures 3 and 4—0.006 A for the HMC sample and 0.004 A for the HM**C**B one, respectively.

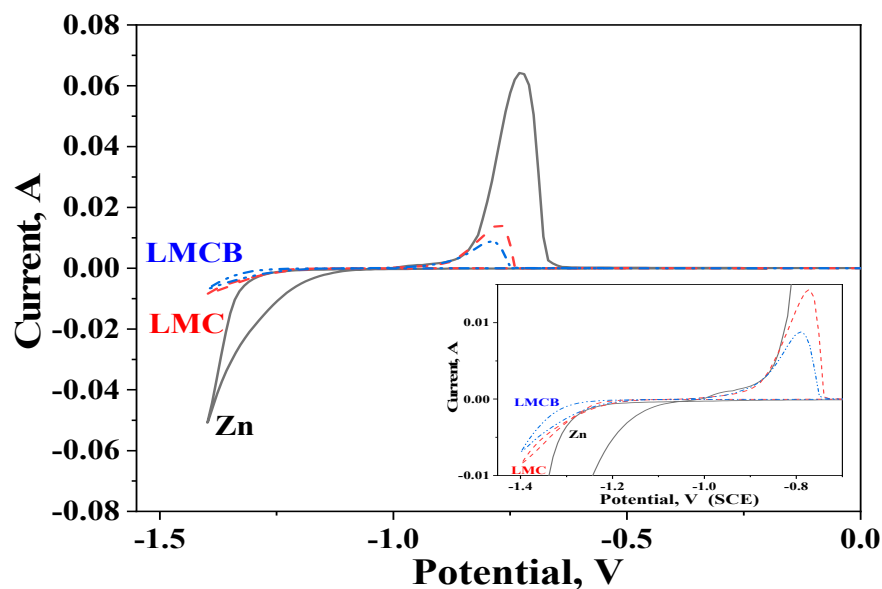


Figure 5. Cyclic voltammetry measurements in starting solutions for hybrid (LMC and LMCB) and ordinary zinc (Zn) coatings.

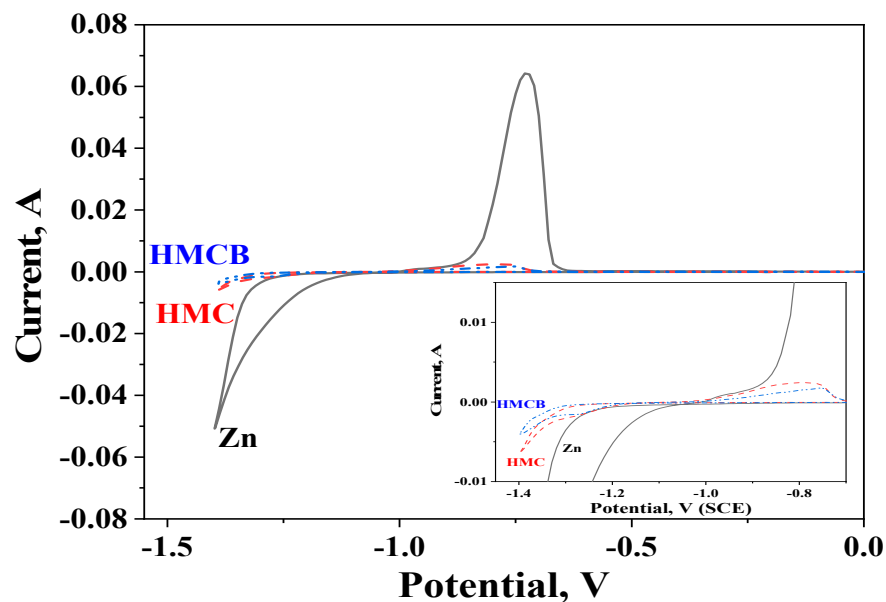


Figure 6. Cyclic voltammetry measurements in starting solutions for hybrid (HMC and HMCB) and ordinary zinc (Zn) coatings.

The Inset in Figure 6 clearly demonstrates the occurring processes. Also here, the reason for such behavior can be explained with the differences in the structure and electrokinetic charge of the polymeric particles used. LMC and LMCB have higher electrokinetic charge, so it could be expected that during the cathodic electrodeposition process these particles will be clamped more tightly to the steel substrate, which will affect the mechanical strength of the coating.

3.6. Potentiodynamic Polarization (PDP) Curves

Potentiodynamic investigations of ordinary zinc and both hybrid coatings (LMC and LMCB, respectively) in the model test medium are presented in Figure 7. Some of the most important electrochemical parameters obtained from the figure are shown in Table 3.

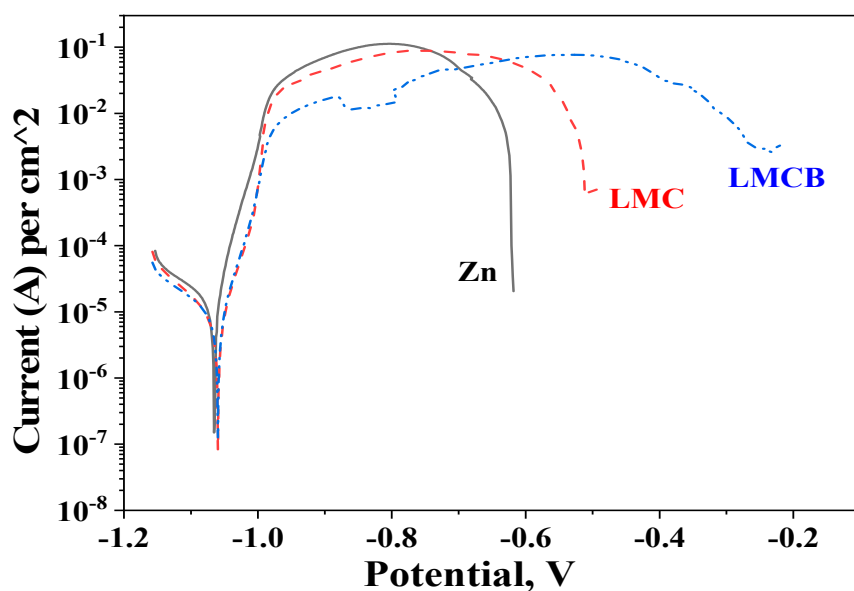


Figure 7. Potentiodynamic polarization curves of ordinary zinc (Zn) and hybrid coatings LMC and LMCB.

Table 3. Electrochemical parameters obtained from Figure 6.

Sample	I_{corr} , $A \cdot cm^{-2}$	E_{corr} , V
Zn	1.7×10^{-5}	-1.07
LMC	7.9×10^{-6}	-1.06
LMCB	8.1×10^{-6}	-1.06

The corrosion potentials of the investigated samples in 5% NaCl solution are very close (see Table 3). However, the corrosion current densities and the shape of the curves differs—the corrosion current density I_{corr} of the zinc is higher while the same parameter of both hybrids is lower. The anodic curve of the ordinary zinc passes through a maximum at potential of about -0.8 V. In addition, the anodic current of this sample increases gradually in the zone after the corrosion potential until the complete dissolution of the coating in the potential area of about -0.6 V and appearing of the steel surface. Both hybrid zinc-based coatings LMC and LMCB demonstrate different behavior. First of all, the anodic parts of these curves are longer compared to that of the Zn, which means that these coatings last longer at conditions of external anodic potential. The length of LMC sample is up to about -0.5 V and that of LMCB is until -0.23 V. The length of the curves is a sign of the full dissolution of the coatings at that condition. In the area of the maximal anodic dissolution, both hybrid samples distinguish with lower maximal current densities in comparison to the zinc.

The main reason for the observed results seems to be the composition of the investigated hybrid coatings as well as the type and quantity of the corrosive products appearing during the test. As is well known from the literature, the expected corrosion product in that test medium is generally zinc hydroxide chloride $Zn_5(OH)_8Cl_2 \cdot H_2O$, which is characterized by a very low product of solubility value [28–32]. Its presence ensures the protection of the low-carbon steel substrate since it partially impedes the penetration of the chloride ions deep inside. The presence of chitosan particles with low polymer weight in the zinc matrix additionally increases the protective ability of the coating leading to the appearance of “barrier effect” for the aggressive ions. In the case when an inhibitor BTA is also included, the protective effect is more clearly presented. This follows from the fact that BTA leaves the particles as a result of the decrease of the pH value during the corrosion process since the shell of the particles is partially or fully ruptured. Thereafter, this inhibitor “outflows”

in the surrounding zone of the particles, improving in such a way the corrosion resistance of the hybrid [31,32].

The situation differs in the case when the hybrid coatings contain HMC or HMCB particles, respectively (Figure 8 and Table 4). It is obvious that the corrosion potentials of the investigated samples are close. However, compared to Figure 6, the corrosion current densities of HMC and HMCB hybrid coatings are lower. Regardless of that, the anodic parts of these curves are much shorter compared to the case of LMC and LMBC particles. This observation means that these hybrid coatings last a shorter time at conditions of external anodic potential in that test medium, and their corrosion resistance is lower. Also here, the length of the coating with BTA is longer compared to the case without inhibitor, but the difference is smaller as opposed to that registered in Figure 7.

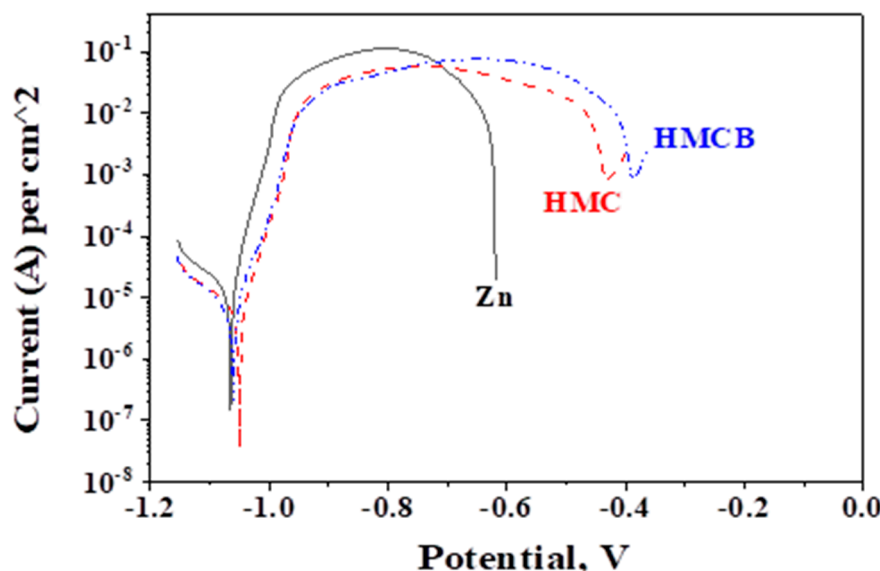


Figure 8. Potentiodynamic polarization curves of ordinary zinc (Zn) and hybrid coatings HMC and HMCB.

Table 4. Electrochemical parameters obtained from Figure 7.

Sample	I_{corr} , $A \cdot cm^{-2}$	E_{corr} , V
Zn	1.7×10^{-5}	-1.07
HMC	6.9×10^{-6}	-1.07
HMCB	6.1×10^{-6}	-1.05

In general, it might be concluded that the presence of chitosan particles with low or high molecular weight positively influences the corrosion characteristics of the ordinary zinc at conditions of external potential, i.e., at accelerated corrosion test. This influence can be registered from the appearance of longer anodic curves and lower corrosion current densities compared to zinc. This observation can be accepted as a sign of their better stability and increased corrosion resistance in a model medium containing chloride ions as corrosion activators. The differences in the anodic behavior of the hybrid coating types could be explained having in mind the ζ -potential values (electrokinetic charge), i.e., the latter exert a noticeable effect. It seems that no other parameter plays a more significant role since the sizes of the chitosan particles are practically equal.

3.7. Polarization Resistance (R_p) Measurements

The results from the polarization resistance measurements have been obtained after stay of 45 days' period of the investigated samples in the model corrosive medium of 5% NaCl solution and are shown in Figure 9 (for LMC and LMBC) and Figure 10 (for HMC

and HMCB), respectively. The samples of the ordinary zinc coating demonstrate on average R_p values of about $800\text{--}850 \text{ ohm}\cdot\text{cm}^2$ during this period. At the beginning of the test, its polarization resistance is $\sim 780 \text{ ohm}\cdot\text{cm}^2$, and at the end of the test period this parameter is almost the same. The maximum of the R_p is received in the middle of the period after 25 days' immersion. The experimental maximal R_p results for LMC ($\sim 1450 \text{ ohm}\cdot\text{cm}^2$) and LM**C**B ($\sim 1700 \text{ ohm}\cdot\text{cm}^2$) demonstrate much higher values (about twice) compared to the ordinary zinc. This means that the presence of the chitosan particles and entrapped BTA positively influence the anticorrosion behavior in that medium, as shown in Figure 9. The impact of the incorporated particles is much more weakly expressed for HMC and HMCB samples, respectively, as shown in Figure 10. According to the obtained results, it is obvious that the ordinary zinc demonstrates the highest polarization resistance until the 35th day of the test. Contrary to this, the R_p values of HMC are much lower during the test, reaching a value of $\sim 720 \text{ ohm}\cdot\text{cm}^2$. Thereafter, this hybrid coating is practically fully dissolved, leaving the low-carbon steel substrate unprotected. For comparison, the HMCB sample also shows lower polarization resistance, but at the end of the immersion period, its values increase up to about $1050 \text{ ohm}\cdot\text{cm}^2$, being however lower than that of LMC and LM**C**B, respectively.

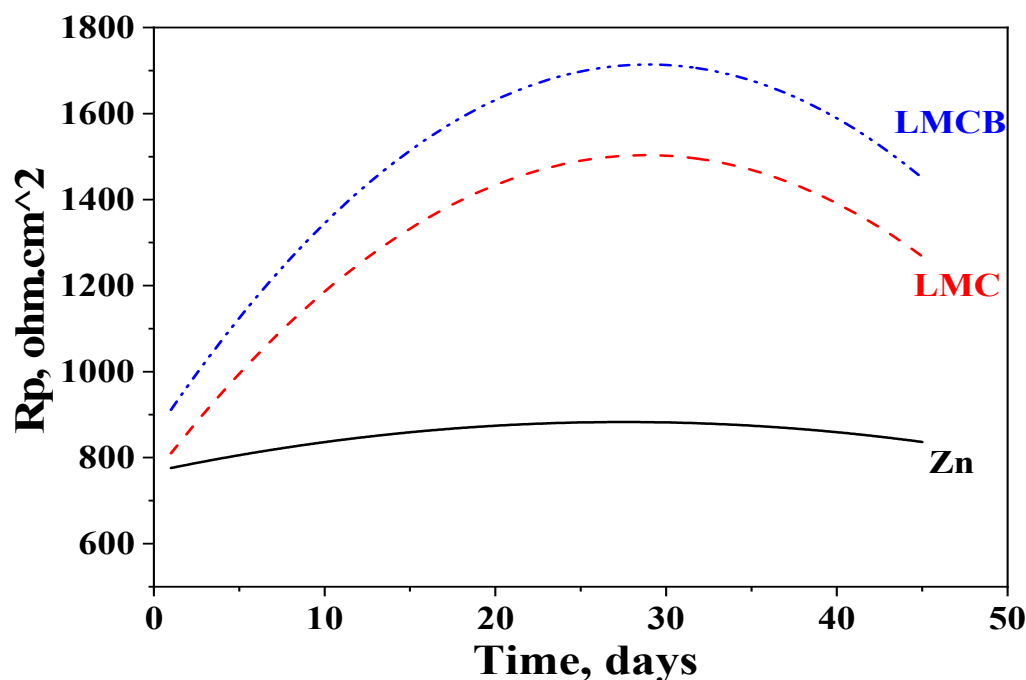


Figure 9. Polarization resistance of ordinary zinc (Zn) and hybrid coatings LMC and LM**C**B.

These results might be explained with the appearance of a layer of corrosion product in that model media, in accordance with our previous studies [28–32]. This is the compound zinc hydroxide chloride (ZHC) with a low product of solubility value, which ensures additional protection against the corrosion activators creating a “barrier” layer. The presence of chitosan particles and BTA improve this effect in the case of LMC and LM**C**B. In the case of HMC and HMCB, such an effect is not registered, and the reason could be the weaker mechanical strength due to different electrokinetic charge (ζ -potential).

However, in the case of the immersion test (“open-circuit” conditions), the forming and appearance of ZHC compound occurs differently contrary to the case of the external polarization (which is the accelerated test). In addition, the composition of the newly formed “mixed” layers seems to differ, leading to some peculiarities in the corrosion behavior.

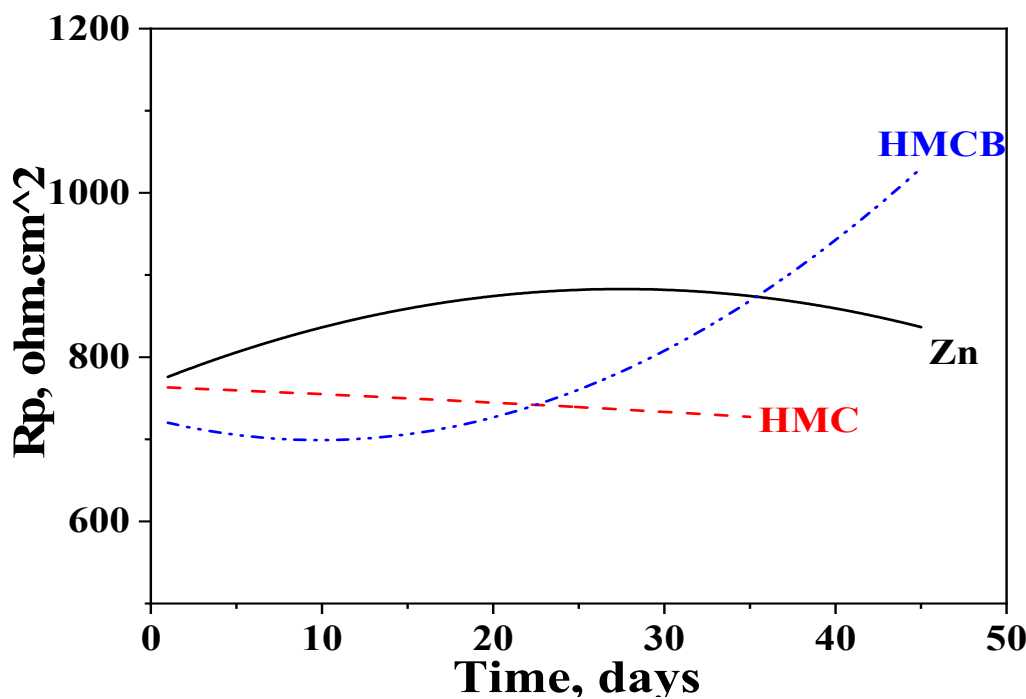


Figure 10. Polarization resistance of ordinary zinc (Zn) and hybrid coatings HMC and HMBC.

3.8. Surface Topography and Wettability

The surface topography images of the prepared hybrid coatings analyzed by AFM are shown in Figure 11. Apparently, the LMC and LMCB coatings show the rough and non-uniform surface of hybrid material containing mainly domains of size 0.5–1.0 μm .

Oppositely, the HMC and HMBC coatings pose a smooth and more uniform surface of hybrid material, enclosing mainly domains of size 0.2–0.4 μm . The roughness values for all coatings are summarized in Table 5, and AFM-obtained results are in agreement with those received from SEM analyses.

Table 5. Roughness parameters from Figure 11.

Sample	LMC	LMCB	HMC	HMBC
Image ($\mu\text{m} \times \mu\text{m}$)	5×5	5×5	5×5	5×5
Rq (nm)	26.1	44.5	11.7	18.1
Ra (nm)	20.7	34.2	8.9	13.2

The AFM tapping mode phase images of the LMC, LMCB, HMC, and HMBC hybrid coatings are additionally presented in Figure 12 below.

The wettability of the hybrid coating surfaces was evaluated by measuring the water contact angle (Figure 13). As seen, water contact angles decrease in order: LMC > HMC > LMCB > HMBC. In addition, water contact angle (WCA) of LMC, HMC, and LMCB was larger than 90° showing hydrophobicity of these coatings. In contrast, HMBC hybrid coating demonstrated WCA less than 90° , which proves their hydrophilicity.

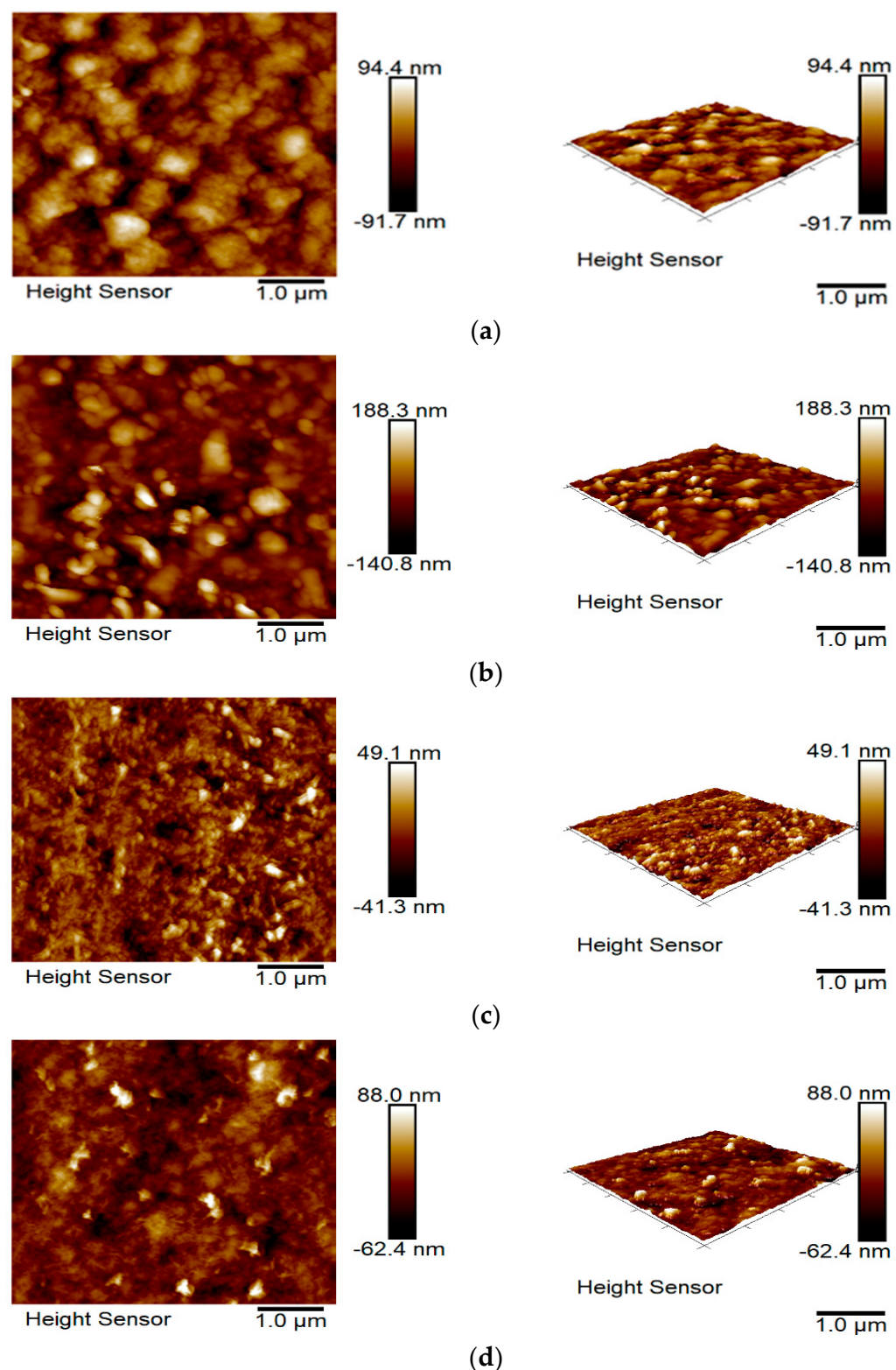


Figure 11. AFM tapping mode 2D and 3D images of the hybrid coatings of: (a) LMC; (b) LMCB; (c) HMC; and (d) HMCB.

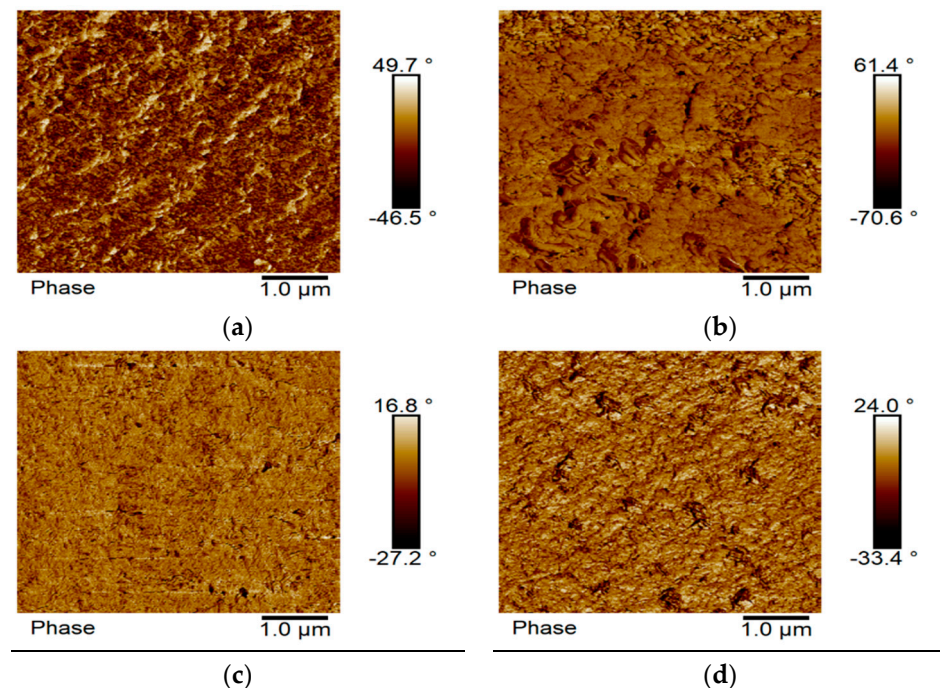


Figure 12. AFM tapping mode phase images of the hybrid coatings of: (a) LMC; (b) LMBC; (c) HMC; and (d) HMBC.

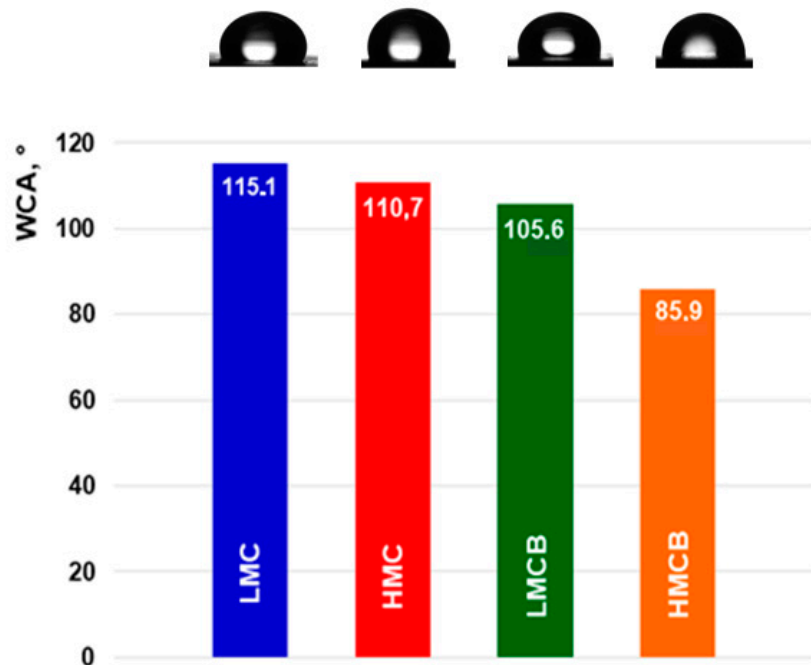


Figure 13. WCA values and representative images of the droplets poured onto hybrid coatings of: LMC (blue); HMC (red); LMBC (green), and HMBC (orange).

4. Conclusions

The successful preparation of hybrid zinc coatings containing particles of low and high molecular weight chitosan with a potential for low-carbon steel protection in aggressive corrosion environment was reported. The application of chitosan-based particles allows the formation of hybrid coatings with nearly homogeneous distribution of the particles from suspensions stabilized against aggregation. SEM and AFM characterization revealed the disposal of many chitosan particles with or without incorporated corrosion inhibitor

BTA near or directly on the coatings surface, which made them able to ensure fast reaction against the corrosive agents. The contact angle measurements proved that the hybrid coatings without entrapped BTA are more hydrophobic compared to those with BTA.

Hybrid zinc coatings LMC and LMCB provided enhanced corrosion protection of low-carbon steel in model medium of 5% NaCl solution for a prolonged period of 45 days. Their protective characteristics are greater compared to the ordinary zinc, most probably because of the appearance of a “mixed” layer consisting of zinc hydroxide chloride (ZHC) and chitosan particles with different molecular weight. This mixed layer ensures a “barrier” effect against the aggressive Cl^- ions presenting in the test solution. The combined anticorrosion effect of chitosan with different physicochemical characteristics and additionally entrapped inhibitor on the corrosion process was studied by the formation of chitosan-based particles loaded with BTA.

The polymer particles were synthesized through an ion-gelation method. It was registered that the hydrodynamic radius of the unloaded (ca. 200 nm) and BTA-loaded particles (ca. 130 nm) do not depend on the chitosan molecular weight. However, the electrokinetic potential of the particles slightly depends on the characteristics of the polymer. It was supposed that the incorporation of the longer molecules of high-molecular-weight polymer into the matrix is suppressed due to conformation effects. As a result, the chitosan concentration in the matrix decreased and the positive charge of the complex is lower compared to the particles formed from low-molecular-weight polymer. The concentration of BTA in the structures was evaluated at ca. 3.71 mg/mL (or EE% is 99%).

Author Contributions: Conceptualization, V.M. and N.B. (Nikolai Boshkov); Data curation, V.M. and N.B. (Nelly Boshkova); Formal analysis, V.M., G.G., O.S., N.B. (Nikolai Boshkov), and N.B. (Nelly Boshkova); Funding acquisition, N.B. (Nikolai Boshkov) and O.S.; Investigation, V.M., N.B. (Nelly Boshkova), G.G., and O.S.; Methodology, V.M., N.B. (Nelly Boshkova), G.G., O.S., and N.B. (Nikolai Boshkov); Writing—review and editing, V.M., G.G., O.S., N.B. (Nelly Boshkova), and N.B. (Nikolai Boshkov). All authors have read and agreed to the published version of the manuscript.

Funding: This work is funded by the European Regional Development Fund within the OP Science and Education for Smart Growth 2014–2020, Project CoE National Center for Mechatronics and Clean technologies, No. BG05M2OP001-1.001-0008.

Institutional Review Board Statement: Not applicable.

Informed Consent Statement: Not applicable.

Data Availability Statement: Data are contained within the article.

Acknowledgments: Research equipment of the Distributed Research Infrastructure INFRAMAT, part of the Bulgarian National Roadmap for Research Infrastructures, supported by the Bulgarian Ministry of Education and Science, was used for some investigations in the present study. The authors thank D. Karashanova for the visualization analysis of the produced structures by Transmission Electron Microscopy.

Conflicts of Interest: The authors declare no conflicts of interest.

References

1. Muzzarelli, R.A.A. *Natural Chelating Polymers: Alginic Acid, Chitin and Chitosan*; Pergamon Press Oxford: New York, NY, USA, 1973; p. 254.
2. Dash, M.; Chiellini, F.; Ottenbrite, R.M.; Chiellini, E. Chitosan—A versatile semi-synthetic polymer in biomedical applications. *Prog. Polym. Sci.* **2011**, *36*, 981–1014. [[CrossRef](#)]
3. Kong, M.; Chen, X.G.; Xing, K.; Park, H.J. Antimicrobial properties of chitosan and mode of action: A state of the art review. *Int. J. Food Microbiol.* **2010**, *144*, 51–63. [[CrossRef](#)] [[PubMed](#)]
4. Hossain, F.; Perales-Perez, O.J.; Hwang, S.; Roman, F. Antimicrobial nanomaterials as water disinfectant: Applications, limitations and future perspectives. *Sci. Total Environ.* **2014**, *466–467*, 1047–1059.
5. Rabae, E.I.; Badawy, M.E.T.; Stevens, C.V.; Smaghe, G.; Steurbaut, W. Chitosan as antimicrobial agent: Applications and mode of action. *Biomacromolecules* **2003**, *4*, 1457–1465. [[CrossRef](#)] [[PubMed](#)]
6. Aranaz, I.; Alcántara, A.R.; Civera, M.C.; Arias, C.; Elorza, B.; Caballero, A.H.; Acosta, N. Chitosan: An Overview of Its Properties and Applications. *Polymers* **2021**, *13*, 3256. [[CrossRef](#)] [[PubMed](#)]

7. Shoueir, K.R.; El-Desouky, N.; Rashad, M.M.; Ahmed, M.K.; Janowska, I.; El-Kemary, M. Chitosan based-nanoparticles and nanocapsules: Overview physicochemical features, applications of a nanofibrous scaffold, and bioprinting. *Int. J. Biol. Macromol.* **2021**, *167*, 1176–1197. [CrossRef] [PubMed]
8. Zhaoa, Q.; Guoa, J.; Cuia, G.; Hana, T.; Wu, Y. Chitosan derivatives as green corrosion inhibitors for P110 steel in a carbon dioxide environment. *Colloids Surf. B Biointerfaces* **2020**, *194*, 111150. [CrossRef] [PubMed]
9. Kong, P.; Feng, H.; Chen, N.; Lu, Y.; Li, S.; Wang, P. Polyaniline/chitosan as a corrosion inhibitor for mild steel in acidic medium. *RSC Adv.* **2019**, *9*, 9211–9217. [CrossRef] [PubMed]
10. Verma, C.; Ebenso, E.E.; Quraishi, M.A.; Hussain, C.M. Recent developments in sustainable corrosion inhibitors: Design, performance and industrial scale applications. *Mater. Adv.* **2021**, *2*, 3806–3850. [CrossRef]
11. Calvo, P.; Remunan-Lopez, C. Novel hydrophilic chitosan-polyethylene oxide nanoparticles as protein carriers. *J. Appl.* **1997**, *63*, 125–132. [CrossRef]
12. Wen, F.; Wei, Y.; Xu, Z.; Ni, H. Formation mechanism of monodisperse, low molecular weight chitosan nanoparticles by ionic gelation technique. *Colloids Surf. B Biointerfaces* **2012**, *90*, 21–27.
13. Mazancová, P.; Némethová, V.; Trelová, D.; Kleščíková, L.; Lacík, I.; Rázga, F. Dissociation of chitosan/tripolyphosphate complexes into separate components upon pH elevation. *Carbohydr. Polym.* **2018**, *192*, 104–110. [CrossRef] [PubMed]
14. De Carvalho, F.G.; Magalhães, T.C.; Teixeira, N.M.; Gondim, B.L.C.; Carlo, H.L.; Dos Santos, R.L.; De Oliveira, A.R.; Denadai, Â.M.L. Synthesis and characterization of TPP/chitosan nanoparticles: Colloidal mechanism of reaction and antifungal effect on *C. albicans* biofilm formation. *Mater. Sci. Eng. C* **2019**, *104*, 109885.
15. Huang, Y.; Lapitsky, Y. Monovalent salt enhances colloidal stability during the formation of chitosan/tripolyphosphate microgels. *Langmuir* **2011**, *27*, 10392–10399. [CrossRef] [PubMed]
16. Koukaras, E.N.; Papadimitriou, S.A.; Bikaris, D.N.; Froudakis, G.E. Insight on the formation of chitosan nanoparticles through ionotropic gelation with tripolyphosphate. *Mol. Pharm.* **2012**, *9*, 2856–2862. [CrossRef] [PubMed]
17. Sreekumar, S.; Goycoolea, F.M.; Moerschbacher, B.M. Parameters influencing the size of chitosan-TPP nano- and microparticles. *Sci. Rep.* **2018**, *8*, 4695. [CrossRef] [PubMed]
18. Popoola, P.A.I.; Malatji, N.; Fayomi, O.S. Fabrication and properties of zinc composite coatings for mitigation of corrosion in coastal and marine zone. In *Applied Studies of Coastal and Marine Environments*; InTech: London, UK, 2016; Volume 32, pp. 137–144.
19. De La Fuente, D.; Castano, J.G.; Morcillo, M. Long-term atmospheric corrosion of zinc. *Corros. Sci.* **2007**, *9*, 1420–1436. [CrossRef]
20. Maniam, K.K.; Paul, S. Corrosion performance of electrodeposited zinc and zinc-alloy coatings in marine environment. *Corros. Mater. Degrad.* **2021**, *2*, 163–189. [CrossRef]
21. Koch, G.; Brongers, M.; Thomson, N.; Virmani, Y.; Payer, J. *Corrosion Cost and Preventive Strategies in the United States*; NACE International: Houston, TX, USA, 2016.
22. Zhang, X.G. *Corrosion and Electrochemistry of Zinc*; Plenum Press: New York, NY, USA, 1996; ISBN 978-1-4757-9877-7.
23. Sorensen, P.A.; Kiil, S.; Dam-Johansen, K.; Weinell, C.E. Anticorrosive coatings: A review. *J. Coat. Technol. Res.* **2009**, *6*, 135–176. [CrossRef]
24. Zhang, H.; Chen, B.; Banfield, J.F. Particle size and pH effects on nanoparticle dissolution. *J. Phys. Chem. C* **2010**, *114*, 14876–14884. [CrossRef]
25. Srivastava, M.; Srivastava, S.K.; Ji, N.G.; Prakash, R. Chitosan based new nanocomposites for corrosion protection of mild steel in aggressive chloride media. *Int. J. Biol. Macromol.* **2019**, *140*, 177–187. [CrossRef] [PubMed]
26. Boshkova, N.; Kamburova, K.; Radeva, T.; Simeonova, S.; Grozev, N.; Shipochka, M.; Boshkov, N. Comparative corrosion characterization of hybrid zinc coatings in Cl⁻-containing medium and artificial sea water. *Coatings* **2022**, *12*, 1798. [CrossRef]
27. Varoqui, R.; Dejardin, P. Hydrodynamic thickness of adsorbed polymers. *J. Chem. Phys.* **1977**, *66*, 4395–4399. [CrossRef]
28. Boshkov, N.; Petrov, K.; Vitkova, S.; Nemska, S.; Raichevski, G. Composition of the corrosion products of galvanic coatings Zn-Co and their influence on the protective ability. *Surf. Coat. Technol.* **2002**, *157*, 171–178. [CrossRef]
29. Boshkov, N.; Petrov, K.; Kovacheva, D.; Vitkova, S.; Nemska, S. Influence of the alloying component on the protective ability of some zinc galvanic coatings. *Electrochim. Acta* **2005**, *51*, 77–84. [CrossRef]
30. Kamburova, K.; Boshkova, N.; Boshkov, N.; Radeva, T. Hybrid zinc coating with CuO nanocontainers containing corrosion Inhibitor for combined protection of mild Steel from corrosion and biofouling. *Coatings* **2022**, *12*, 1254. [CrossRef]
31. Kamburova, K.; Boshkova, N.; Boshkov, N.; Radeva, T. Composite coatings with polymeric modified ZnO nanoparticles and nanocontainers with inhibitor for corrosion protection of low carbon steel. *Colloids Surf. A Physicochem. Eng. Asp.* **2021**, *609*, 125741. [CrossRef]
32. Kamburova, K.; Boshkova, N.; Boshkov, N.; Atanassova, G.; Radeva, T. Hybrid zinc coatings for corrosion protection of steel using polyelectrolyte nanocontainers loaded with benzotriazole. *Colloids Surf. A* **2018**, *559*, 243–250. [CrossRef]

Disclaimer/Publisher's Note: The statements, opinions and data contained in all publications are solely those of the individual author(s) and contributor(s) and not of MDPI and/or the editor(s). MDPI and/or the editor(s) disclaim responsibility for any injury to people or property resulting from any ideas, methods, instructions or products referred to in the content.